N-terminal lipid conjugation of amyloid β(1−40) leads to the formation of highly ordered N-terminally extended fibrils†

Juliane Adler,[a] Holger A. Scheidt,[a] Katharina Lemmnitzer,[a] Martin Krueger[b] and Daniel Huster*[a]

Fibril formation of amyloid β(1−40) (Aβ(1−40)) peptides N-terminally lipid modified with saturated octanoyl or palmitoyl lipid chains was investigated. Lipid modification of Aβ(1−40) significantly accelerates the fibrillation kinetics of the Aβ peptides as revealed by ThT fluorescence. Electron microscopy and X-ray diffraction results indicate a heterogeneous cross-β structure of the fibrils formed by the lipid-conjugated peptides. Solid-state NMR was used to investigate structural features of these fibrils. The lipid moieties form dynamic and loosely structured heterogeneous lipid assemblies as inferred from ^{2}H NMR of the deuterated lipid chains. ^{13}C NMR studies of selected isotopic labels reveals that in addition to Phe_{19} and Val_{39}, which are part of the canonical cross-β structure, also N-terminal residues (Ala_2, Phe_4, Val_{12}) are found in β-strand conformation. This suggests that the increased hydrophobicity induced by the lipid modification, alters the energy landscape rendering an N-terminal extension of the β-sheet structure favorable. Furthermore, the fibrils formed by the Aβ–lipid hybrids are much more rigid than wildtype Aβ fibrils as inferred from NMR order parameter measurements. Taken together, increasing the local hydrophobicity of the Aβ N-terminus results in highly ordered but heterogeneous amyloid fibrils with extended N-terminal β-sheet structure.

1 Introduction

Hybrid molecules that combine two rather different chemical and/or physical properties represent the basis for innovative developments in material science, biotechnology, and even medical applications such as tissue engineering. Among many other examples, the covalent linkage of biological proteins with synthetic polymers has been of high interest in several fields of tissue engineering,[1] drug delivery,[2] and nanotechnology[3] as these new materials display numerous favorable properties. Each component of such molecules displays specific chemical and physical properties that give rise to a defined structure forming process. Often, the combination of two polymers with rather different properties creates an interesting situation where two structure forming principles compete. Tuning the properties of either side of the hybrid molecule, the equilibrium can be shifted towards the dominant mechanism for structure formation. Thus, important insights into the thermodynamics of these processes can be found and an interesting thermotropic phase behavior of such hybrids has been reported.[4]

Peptide–polymer conjugates represent an interesting class of such hybrid molecules. They combine the wealth of the thermotropic structural polymorphism of (synthetic) polymers with the biologically important process of protein structure formation usually referred to as folding. In addition to native protein folding into the active state, misfolding into amyloid structures is observed for both intrinsically disordered and well-folded proteins.[5] Amyloid formation is a self-organization process that many proteins and peptides of very different structural features can undergo leading to ordered aggregates that are characterized by a relatively generic cross-β structure[6,7] that is typically very well defined.[8–10] Synthetic polymers can also assemble into multiple structures, which include, for instance, coiled structures, amorphous and highly ordered crystalline phases, as well as a multitude of curved (micellar, hexagonal, inverse hexagonal) or lamellar structures. Structure formation of polymers is governed by straightforward thermodynamics.[11,12]

Amyloid–polymer hybrids hold great potential for understanding some underlying questions of structure formation. The perhaps most simple polymer modification of proteins is the attachment of poly(ethylene glycol), also called PEGylation, which is also applied in several protein-based medicines to mask a therapeutic protein or drug delivery system from the immune response of the host.[13] In basic research, conjugation of amyloid forming peptides with PEG provides insights into

[a] *Institute for Medical Physics and Biophysics, Leipzig University, Härtelstr. 16-18, 04107 Leipzig, Germany. E-mail: daniel.huster@medizin.uni-leipzig.de; Fax: +49 (0)341 9715709; Tel: +49 (0)341 9715701*

[b] *Institute for Anatomy, Leipzig University, D-04103 Leipzig, Germany*

† Electronic supplementary information (ESI) available. See DOI: 10.1039/c6cp05982a

This journal is © the Owner Societies 2017

Phys. Chem. Chem. Phys., 2017, **19**, 1839–1846 | 1839

the structure forming properties of these hybrids. Previous work has focused on the assembly properties of shorter fragments of amyloid β (Aβ) peptides, C-terminally conjugated with PEG[14–18] or N-terminally with poly(N-isopropylacrylamide) and poly(hydroxyethylacrylate).[19] These studies found a predominance of β-sheet structures, but also coiled coils[19] or spherulite structures[14] have been observed suggesting that other structure forming processes and principles can interfere with amyloid formation. PEG–Aβ hybrids represent interesting model systems to study the competition of PEG crystallization and peptide secondary structure formation.[14] Depending on the length of the PEG chain and the respective peptide segment, both the presence or absence of the characteristic cross-β structure has been confirmed.[14]

Covalent lipid attachment is a biologically occurring mechanism of protein modification typically encountered when otherwise soluble proteins obtain a propensity to bind to lipid membrane surfaces.[20–22] Lipid chains can also be viewed as simple short hydrophobic polymers. Protein–lipid conjugates, therefore, represent interesting hybrid systems that allow addressing fundamental questions of amyloid structure formation. Although none of the biologically relevant proteins that form amyloids are reported to undergo lipid modification *in vivo*, lipidation locally increases the hydrophobicity of the biological copolymer. This allows addressing the question if the self-assembly reaction of amyloid formation is governed by the hydrophobic effect and increased entropy upon water desolvation[9] or requires very specific interactions between residues that result in structural motifs suggestive of a tight, dry steric fit between a pair of sheets that represents the fundamental feature of amyloid fibrils as first highlighted for short peptide sequences ("steric zipper").[23] While general alteration of the hydrophobicity in the β-sheet core of the Aβ sequence resulted in moderate changes in the fibrillation kinetics and local structure and dynamics,[24,25] the more recently published highly resolved solid-state NMR structures of Aβ(1–42) provide strong evidence for rather specific interactions on the single residue scale.[8–10] However, this is only true for the well-ordered part of the Aβ fibrils, which starts at around residue 15.

Full length Aβ peptides carrying an N-terminal polymer or lipid conjugation have not been studied so far. Here, we describe Aβ(1–40) peptides conjugated with saturated C8:0 (octanoyl) or C16:0 (palmitoyl) lipid chains on the N-terminus. This modification serves three purposes: (i) the hydrophobic lipid tail locally increases the hydrophobicity of the Aβ molecule by $\Delta G^0 = -5.8$ and -12.4 kcal mol^{-1} for octanoyl and palmitoyl residues, respectively,[26,27] which should influence the fibrillation kinetics and possibly the extent of the cross-β structure formed. (ii) Lipids are known to show a rich thermotropic phase behavior that results in the assembly into micelles, (inverse) hexagonal structures, or bilayers, which could interfere with amyloid structure formation. This poses the question which structure forming process dominates – peptide amyloid or lipid structure formation. (iii) The lipid modification and the cross-β core of Aβ peptides are linked by the charged and rather hydrophilic N-terminus of the molecules, which has no fibrillating properties and was found to be highly dynamic in solid-state NMR studies.[8,28] This raises the question if the two structure forming principles may progress independent of each other or lead to new structural features.

2 Experimental procedures

2.1 Peptide synthesis

Aβ(1–40) peptides (octanoyl- or palmitoyl-D**A**E**F**RHD**S**GY E**V**HH QKLVFF AEDV**G**SNK GA IIGLMVGG**V**V) were synthesized using standard Fmoc solid phase synthesis. Uniformly ^{13}C/^{15}N-labelled amino acids (Euriso-TOP, Saarbrücken, D) were introduced at positions Ala$_2$, Phe$_{19}$, Gly$_{25}$, Val$_{39}$ (shown in bold and underscored above). A second N-palmitoylated Aβ(1–40) peptide was synthesized with isotopic ^{13}C/^{15}N-labels in position Phe$_4$, Ser$_8$, Gly$_9$, and Val$_{12}$ (shown in italic and underscored in the peptide sequence above). Perdeuterated octanoic-d_{15} or palmitic-d_{31} acid (Euriso-TOP) were coupled to the N-terminus in the final coupling step in peptide synthesis.

2.2 Sample preparation

Lyophilized peptides were solubilized in 25 mM phosphate buffer (pH 7.4) containing 150 mM NaCl and 0.01% NaN$_3$ at a concentration of 1 mg ml^{-1}. For equilibration, the sample was subjected to heating–shaking cycles for at least 45 min by placing the samples in a water bath of 65 °C for 5 min followed by rapid vortexing for 30 seconds. Peptide solutions were then incubated at 37 °C and shaken at 450 rpm for 14 days.

2.3 Determination of the critical micelle concentration

DPH fluorescence was used to determine the critical micelle concentration (CMC) of octanoic and palmitic acid as well as the palmitoyl–Aβ(1–40)-hybrids. Samples for CMC determination were prepared as described in the literature.[29] 1 µl of a 10 mM DPH stock solution (dissolved in THF) were added to varying concentrations of the fatty acids (total volume of 2 ml) and the amyloid fibrils (total volume of 150 µl) in sample buffer. Preheating to 65 °C was necessary to dissolve the fatty acids completely.[30] Tubes were incubated in the dark for 30 minutes at 65 °C. Volumes of 150 µl were pipetted into wells of a 96 well plate and the plate was placed in a Tecan infinite M200 microplate reader (Tecan Group AG, Männedorf, Switzerland). The excitation wavelength was 358 nm and the emission wavelength was 430 nm. Data were fitted with Boltzmann sigmoidal growth function to determine the CMC.

2.4 ThT fluorescence measurements

The fibrillation behavior of the lipid conjugated peptides was studied by fluorescence intensity measurements. Thioflavin T (ThT) was used as a fluorescent dye, which shows increased fluorescence intensity at 482 nm when bound to fibrils displaying the cross-β structure.[31] Experiments were performed in a 96 well plate format. Buffer conditions for fibrillation were the same as described above with additional 20 µM ThT in the incubation solution. After the treatment described in the sample preparation section, volumes of 150 µl were pipetted into the wells and the plate was placed in the Tecan infinite M200 microplate reader. The temperature was set to 37 °C and a shaking cycle of 5 min

1840 | *Phys. Chem. Chem. Phys.*, 2017, **19**, 1839–1846

This journal is © the Owner Societies 2017

shaking (1 mm shaking amplitude and 173.9 rpm) followed by a 5 min waiting time was applied. The fluorescence excitation wavelength was set to 450 nm and the emission was measured at 485 nm. The fluorescence intensity was measured in intervals of 30 min. For comparison, also the kinetics of wildtype of Aβ(1–40) was measured under the same conditions as described above. Data was analyzed using procedures as described in the literature.[32] To slow down the fibrillation kinetics, an altered protocol was applied (2 s of shaking (at 2 mm shaking amplitude), 5 min waiting, 2 s shaking, 5 min waiting, 2 s shaking).

2.5 X-ray diffraction measurements

For X-ray diffraction measurements, fibril samples were placed on nylon loops (Hampton Research, Aliso Viejo, CA, USA) and mounted onto the goniometer head of an X-ray source (Rigaku copper rotating anode MM007 with 0.8 kW, Tokyo, Japan). The signals were recorded using an image plate detector (Rigaku, Tokyo, Japan) with an exposure time of 180 s at room temperature.

2.6 Scanning transmission electron microscopy (TEM)

The general morphology of all fibrils obtained was determined by scanning transmission electron microscopy (TEM). Fibril solutions were diluted 1:20 with pure water. 1 μl droplets of this solution were applied on formvar coated copper grids, allowed to dry for about 1 hour and negatively stained with 1% uranyl acetate in pure water. Transmission electron micrographs were recorded using Zeiss SIGMA, (Zeiss NTS, Oberkochen, Germany) equipped with a STEM detector and Atlas Software.

2.7 Solid-state NMR spectroscopy

For NMR measurements, fibril solutions were ultracentrifuged at 86 000 × g for 2 h at 4 °C. Pellets were lyophilized, rehydrated to 50 wt% deuterium depleted water and homogenized by freezing in liquid nitrogen and thawing at 37 °C. Subsequently, samples were centrifuged into 3.2 mm MAS rotors for MAS NMR or glass vials for static ^{2}H NMR measurements.

^{2}H NMR spectra were acquired on a Bruker Avance I 750 MHz NMR spectrometer (Bruker Biospin GmbH, Rheinstetten, Germany) operating at a resonance frequency of 115.1 MHz for ^{2}H. A single-channel solids probe equipped with a 5 mm solenoid coil was used. The ^{2}H NMR spectra were accumulated with a spectral width of ±250 kHz using quadrature phase detection. A phase-cycled quadrupolar echo sequence[33] was used. The typical length of a 90° pulse was 2.7 to 3.0 μs, the interpulse delay was 30 μs, and a relaxation delay of either 1 s or 50 s was applied.

Magic-angle spinning (MAS) NMR spectra were acquired on a Bruker 600 Avance III NMR spectrometer (Bruker BioSpin GmbH, Rheinstetten, Germany) operating at a resonance frequency of 600.1 MHz for ^{1}H, 150.9 MHz for ^{13}C and 60.8 MHz for ^{15}N. A triple channel 3.2 mm MAS probe was used. Typical pulse lengths were 4 μs for ^{1}H and ^{13}C and 5 μs for ^{15}N. ^{1}H–^{13}C and ^{1}H–^{15}N contact time were 1 ms at a spin lock field of ∼60 kHz, and the relaxation delay 2.5 s. ^{1}H dipolar decoupling during acquisition with an rf amplitude of 70 kHz was applied using Spinal64.

^{13}C–^{13}C DARR and ^{13}C–^{15}N correlation spectra were acquired simultaneously using dual-acquisition.[34] In the same experiment, two-dimensional ^{13}C–^{13}C DARR NMR spectra with mixing times of 100 ms or 600 ms with 128 data points and four ^{15}N–^{13}Cα correlation spectra with 32 data points in the indirect dimensions were acquired. The MAS frequency was 11 777 Hz.

^{1}H–^{13}C coupling constants were measured using the constant time DIPSHIFT experiments.[35] Homonuclear decoupling during dipolar evolution was achieved by applying the frequency switched Lee-Goldberg (FSLG)[36] scheme with an effective radio-frequency field of 80 kHz. The MAS frequency was 5 kHz. The strength of the dipolar coupling was determined from the dephasing curves for each resolved carbon atom by analyzing them with numerical simulations and dividing the result by the rigid limits.[37,38]

All NMR spectra were acquired at a temperature of 30 °C.

3 Results

3.1 Fibrillation kinetics

The fibrillation kinetics of the lipidated Aβ(1–40) hybrids was recorded using the standard ThT assay. A graph displaying the ThT fluorescence intensity as a function of time for wildtype Aβ(1–40), octanoyl–Aβ(1–40), and palmitoyl–Aβ(1–40) is shown in Fig. 1. Sample preparation prior to starting the fluorescence measurements takes about 45 min, which represents the dead time of the ThT assay as samples had to undergo several heating–cooling circles to dissolve. Therefore, the first data points reporting the very fast nucleation are missing in the fluorescence intensity graphs. Wildtype Aβ(1–40) shows the typical ThT fluorescence intensity increase, which can be described by a sigmoidal curve.[39] The characteristic time at which the fluorescence reaches the half maximum ($t_{1/2}$) is 9.6 h for this sample. It is clearly seen that both, octanoyl- and palmitoyl-conjugated Aβ(1–40) peptides undergo accelerated fibrillation.
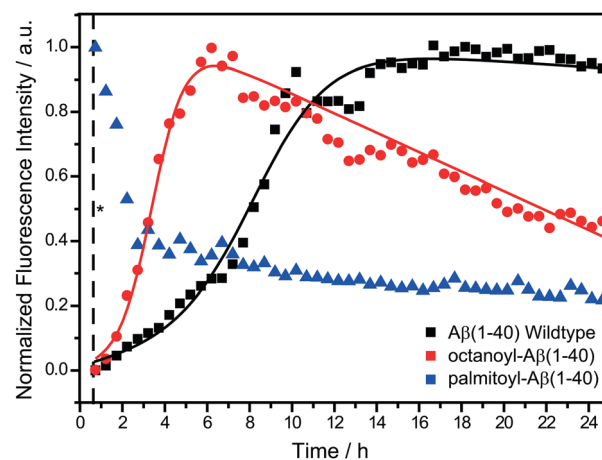

Fig. 1 Thioflavin T (ThT) fluorescence intensity of Aβ(1–40) wildtype (black), octanoyl–Aβ(1–40) (red) and palmitoyl–Aβ(1–40) (blue) as a function of time. The asterisk at 45 minutes indicates the beginning of the fluorescent measurement after prior sample treatment (shaking and heating). Data were fitted using functions discussed in the literature.[39]

This journal is © the Owner Societies 2017

Phys. Chem. Chem. Phys., 2017, 19, 1839–1846 | 1841

The data indicates that fibrillation of the long-chain palmitoyl–Aβ(1–40) is already completed in the dead time of the measurement (∼45 min) and the recorded fluorescence intensity only decreases. This could also be induced by formation of prefibrillar aggregates during preparation. The decreased ThT fluorescence intensity might be caused by sedimentation of the Aβ hybrids in the well plate. As fibrillation of palmitoyl–Aβ(1–40) is very rapid, no lag time or characteristic time could be determined; both must be shorter than 45 min. An increase in ThT fluorescence could not be detected for palmitoyl–Aβ(1–40) even at lower peptide concentration and a preparation protocol involving much less shaking. For the octanoyl–Aβ(1–40), a clearly faster fibrillation kinetics is observed, expressed by $t_{1/2} = 5.5$ h.

We also carried out ThT fluorescence kinetics measurements of wildtype Aβ(1–40) peptides in the presence of equimolar concentration of octanoic and palmitic acid, respectively, shown in Fig. S1 (ESI†). The CMC of the free fatty acids was determined to be 54.1 μM for palmitic acid and 50.6 mM for octanoylic acid, so the peptide concentration of 230 μM used in the measurements was in between these values. In the presence of equimolar concentrations of octanoic acid the lag time of wildtype Aβ(1–40) fibrillation is decreases by ∼45%, while only a moderate effect was observed in the presence of 230 μM palmitic acid (lag time reduced by ∼3%).

3.2 Fibril morphology investigated by TEM and X-ray diffraction

The electron microscopy images of the lipid-conjugated Aβ peptides reported in Fig. 2 show typical long unbranched amyloid fibrils with diameters of $d = (18.6 \pm 5.9)$ nm for octanoyl–Aβ(1–40) and (16.8 ± 3.5) nm for palmitoyl–Aβ(1–40). The diameter as well as its variation are larger than for the wildtype Aβ(1–40) fibrils that have been reported to exhibit a mean diameter of (10.0 ± 1.6) nm.[24] This indicates a higher heterogeneity for the fibrils formed by the lipid-conjugated Aβ(1–40) peptides.

X-ray diffraction images show the two typical reflections of the cross-β structure of amyloid fibrils, with one sharp reflection describing a fixed distance of 4.7 Å, which defines the interstrand hydrogen bond distance and one broad peak, which characterizes the intersheet distance of the opposing β-strands.[40] The X-ray diffraction pattern of wildtype and lipid-conjugated Aβ(1–40) are displayed in Fig. S2 of the ESI.† The width of the reflections is an indication of heterogeneity of the fibrils. The broad reflections indicate intersheet distances of 11.0 Å for octanoyl–Aβ(1–40) and 10.2 Å for palmitoyl–Aβ(1–40). These reflections are much broader for the lipid-conjugated Aβ peptide fibrils indicating higher heterogeneity and possibly structural polymorphism.

3.3 Secondary structure of lipid-conjugated Aβ(1–40) fibrils

It is important to investigate if the characteristic structure of the Aβ fibrils is retained in the fibrils formed by lipid-modified Aβ conjugates. To obtain insights into the secondary structure of the amyloid fibrils formed from the lipid-conjugated Aβ(1–40) peptides, ¹³C and ¹⁵N solid-state MAS NMR spectra were recorded. The assignments of the signals of the four aforementioned ¹³C/¹⁵N labelled amino acids were carried out by means of
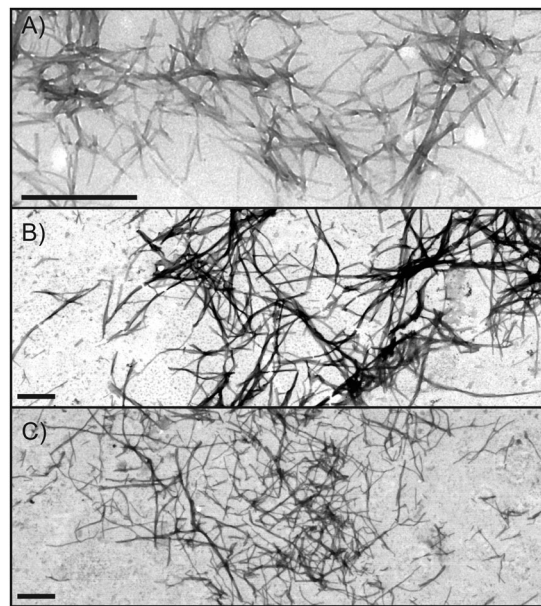

Fig. 2 Transmission electron micrographs of fibrils of wildtype Aβ(1–40) (A), octanoyl–Aβ(1–40) (B), and palmitoyl–Aβ(1–40) (C). The scale bar represents 500 nm.

co-acquisition of ¹³C–¹³C DARR and ¹³Cα–¹⁵N correlation NMR experiments.[34] All ¹³C and ¹⁵N chemical shifts of the labeled nuclei are listed in Table S1 of the ESI,† along with characteristic NMR spectra (Fig. S3 and S4, ESI†). The NMR signals are relatively broad for the lipid conjugated peptides confirming the more heterogeneous and polymorphous nature of these fibrils compared to those assembled from wildtype Aβ peptides. As known from empirical correlations, ¹³C NMR chemical shifts are directly related to the local secondary structure in proteins.[41] Fig. 3 displays the correlation of these chemical shifts with local secondary structure. Calibration independent differences of the ¹³Cα and ¹³Cβ signals are reported for Ala₂, Phe₁₉, and Val₃₉, while the absolute value of the ¹³CO chemical shift of Gly₂₅ is provided. The bars represent the mean chemical shift values obtained for α-helix, random coil, and β-sheet. For wildtype Aβ(1–40) fibrils, β-sheet chemical shifts are obtained for Phe₁₉, Gly₂₅, and Val₃₉, while Ala₂ is found in random coil structure in agreement with the literature.[28] No large chemical shift changes of residues Phe₁₉, Gly₂₅, and Val₃₉ are observed for both types of lipid-conjugated Aβ(1–40) fibrils. However, the N-terminal residue Ala₂ showed a drastic chemical shift change of more than −5 ppm for both lipid-conjugated Aβ peptides, indicating that this residue also resides in a β-sheet secondary structure. This suggests that the β-sheet secondary structure is extended to the N-terminus. For Ala₂, the Cα–Cβ crosspeak indicates that some fraction (50% for palmitoyl–Aβ(1–40) and 26% for octanoyl–Aβ(1–40)) is also found in non-β-sheet like chemical structure confirming the heterogeneous nature of the obtained fibrils (Fig. S4, ESI†).

To further investigate the possible N-terminal extension of the fibrillar structure of lipid conjugated Aβ(1–40) fibrils, an additional palmitoylated-Aβ(1–40) peptide variant with isotopic labels in positions Phe₄, Ser₈, Gly₉, and Val₁₂ was prepared.
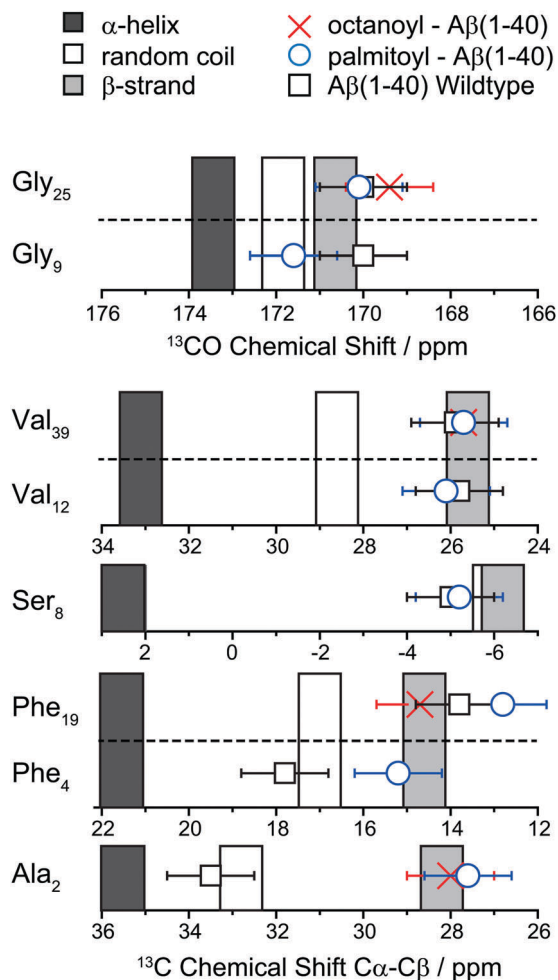
Fig. 3 Overview of the local secondary structure of the labelled amino acids Ala$_2$, Phe$_{20}$, Gly$_{25}$, and Val$_{39}$ of the conjugated peptides derived from the ^{13}C NMR chemical shifts. Plotted are the ^{13}Cα–^{13}Cβ chemical shift changes for Ala$_2$, Phe$_{20}$, and Val$_{39}$ as well as the absolute ^{13}CO chemical shift of Gly$_{25}$. A second set of N-terminal chemical shift values is given for palmitoyl–Aβ(1–40) including residues Phe$_4$, Ser$_8$, Gly$_9$, and Val$_{12}$. The bars represent the reference values of α-helix, random coil and β-sheet secondary structure as reported in the literature.[41] Experimental data is given as black squares for Aβ(1–40) wildtype, red crosses for octanoyl–Aβ(1–40), and as blue circles for palmitoyl–Aβ(1–40).

All these isotopic labels were concentrated in the N-terminus. The solid-state NMR chemical shifts of these amino acids are also shown in Fig. 3 and Table S1 (ESI†). Confirming the results for Ala$_2$, β-sheet structure was also found for Phe$_4$ and Val$_{12}$. The chemical shift of Gly$_9$ is random coil, while chemical shift data for Ser$_8$ is not conclusive as chemical shift data of serine in random coil and β-sheet secondary structure is indistinguishable.[41]

3.4 Structural features of the lipid modifications of Aβ(1–40)

^{2}H NMR is a well-established method to characterize the thermotropic phase behavior of lipids, allowing to distinguish between different phases.[42,43] Static ^{2}H NMR spectra of the fibrils formed of octanoyl-d_{15}–Aβ(1–40) and palmitoyl-d_{31}–Aβ(1–40) are shown in Fig. 4. The spectral line shape is best described as
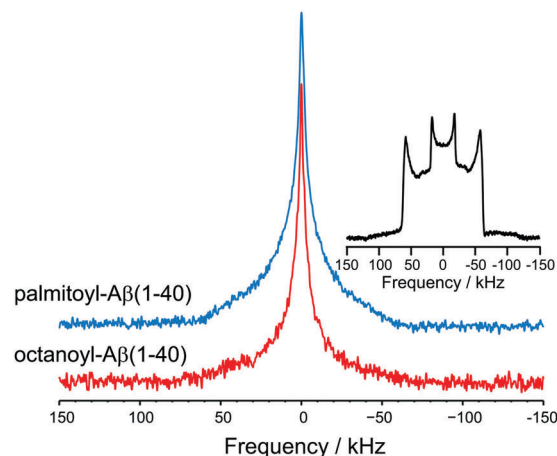

Fig. 4 Static ^{2}H NMR spectra of octanoyl-d_{15}–Aβ(1–40) (red) and palmitoyl-d_{31}–Aβ(1–40) (blue). The inset shows the ^{2}H NMR spectrum of palmitic acid-d_{31}.

Super-Lorentzian without any resolved Pake doublets or other clear characteristic features. But the base of the ^{2}H NMR lines is very broad well exceeding 50 kHz. This is a strong indication that the chains are heterogeneous and loosely structured. Motions occur on intermediate timescales and feature varying amplitudes. However, no well-ordered structure of the lipid moieties if formed and some of the segments also appear to be isotropic. For comparison, the ^{2}H NMR spectrum of pure palmitic acid-d_{31} is shown, which has two contributions from the rigid chain methylenes and the rotating terminal methyl group, exhibiting quadrupolar splittings of ∼122 and 40 kHz, respectively, in agreement with previously published data.[44]

3.5 Motional amplitudes of lipid-conjugated Aβ(1–40) fibrils

Finally, ^{1}H–^{13}C dipolar coupling measurements using the DIPSHIFT NMR experiment were carried out to obtain information about the molecular dynamics of the individual segments of the lipid-modified Aβ(1–40) peptides. As the ^{1}H–^{13}C dipolar couplings are motionally averaged, the ratio of the averaged and the full dipolar coupling reports an order parameter that is indicative of the amplitude of motion of the respective C–H bond. These order parameters are plotted for all labeled segments of the investigated Aβ fibrils in Fig. 5.

In general, the fibrils formed by the lipid-conjugated Aβ(1–40) peptides showed higher order parameters than wild-type Aβ(1–40) fibrils indicative of more compact packing of the individual molecular segments. The most pronounced ordering is observed for residues Ala$_2$ and Phe$_4$, which also showed the most drastic secondary structure change. While in wildtype Aβ(1–40) fibrils, the N-terminus is unstructured and relatively mobile,[28] lipid conjugated Aβ(1–40) peptides form fibrils where the N-terminus is in β-sheet structure that is more restricted expressed by higher order parameters, which is also in agreement with the β-sheet structure found for Ala$_2$ and Phe$_4$. Most other residues show slightly higher order parameters, but the differences lie within experimental error of the measurement.
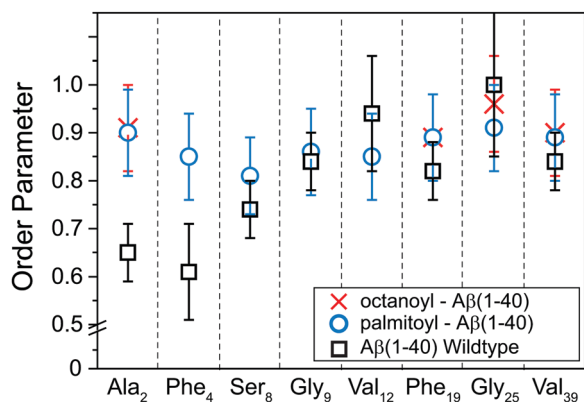
Fig. 5 ^{1}H–^{13}C order parameters of the individual segments of the labeled amino acids of the amyloid fibrils of the peptide–lipid chain hybrids. Experimental data is given by as black squares for Aβ(1–40) wildtype, red crosses for octanoyl–Aβ(1–40), and as blue circles for palmitoyl–Aβ(1–40).

4 Discussion

The hydrophobic effect and entropy gain of desolvated water upon fibril formation are considered the major driving forces for amyloid formation.[9] While a well-structured cross-β core exists for Aβ,[8–10] the N-terminal part has been reported to be relatively flexible showing essentially no secondary structure.[28] N-terminal lipid modification of Aβ(1–40) (i) significantly accelerates the fibrillation kinetics, (ii) induces β-sheet structure in the N-terminus, and (iii) results in a significant ordering of the N-terminus and the entire fibrils.

All these effects can be explained by the increased hydrophobicity of Aβ induced by the lipidated N-terminus. In aqueous environment, lipid chains have a high propensity to assemble to form structures such as micelles or bilayers. We determined the CMC of palmitic and octanoic acid to be 54.1 μM and 50.6 mM, respectively. Fibrillation experiments of the lipid-conjugated Aβ peptides were done at a peptide concentration of 230 μM, which is above the CMC of palmitic acid and much below the CMC of octanoic acid. This may explain why palmitoyl–Aβ(1–40) showed very fast amyloid forming kinetics as prefibrillar micellar aggregates may form instantaneously. Furthermore, even though the octanoyl–Aβ(1–40) concentration was much below the CMC, still the fibrillation kinetics was faster suggesting that the increase in hydrophobicity does indeed contribute to the fibrillation kinetics.

Our data suggest that the N-terminal lipid modifications of Aβ also form some loosely structured heterogeneous lipid assembly, which is however rather dynamic. However, there are no bilayer or hexagonal lipid phases formed. Clearly, this tendency also helps to associate the hybrid molecules to form Aβ fibrils as indicated by much accelerated fibrillation kinetics. Likely, N-terminal lipid modifications decrease the energy barrier separating the unstructured and the amyloid states. The lipids of the N-terminal part of the lipidated Aβ peptides are dynamic and loosely associated as indicated by the ^{2}H NMR spectra of the deuterated lipid modifications. We did not detect the well-known superposition of ^{2}H NMR Pake spectra with varying quadrupolar splittings as known from liquid crystalline

membranes or inverse hexagonal lipid structures.[42] Rather, the observed Super-Lorentzian lineshape of the ^{2}H NMR spectra of the lipid chains indicates that the lipid moieties in the aggregated structures undergo multiple conformational transitions on a fast and intermediate time scale. As oppose to free lipid micelles in aqueous solution, the N-terminal lipid modifications linked to Aβ peptides cannot undergo fast diffusion on the highly curved micellar surface; neither can the micelles tumble freely in solution as they are constraint by the amyloidic peptide segments. As a consequence, the NMR line at half maximum is rather broad (~6.5 kHz), which is clearly much higher than what is known for free detergent micelles.[45] A residual quadrupolar splitting of 6.5 kHz would correspond to a ^{2}H NMR order parameter of 0.05. This is much lower than the 0.65 that has been reported for the first amino acid of unmodified Aβ(1–40).[28] However, as spectral intensity spreads out up to widths of >50 kHz, also relatively ordered lipid segments are present in these preparations emphasizing the very high gradient in the segmental dynamics of these lipid assemblies.

Very short fibril forming dipeptides with N-terminal lipid modifications have been studied before.[46] These peptides formed well-ordered fibrils and the lipid modifications were found in a crystalline structure as if they were part of the fibril.[46] Clearly, lipid modified Aβ(1–40) peptides form more heterogeneous assemblies and are not part of a highly ordered structure. As the morphological data (electron microscopy, X-ray diffraction) as well as the fact that the NMR measurements indicate several polymorphs suggest, fibrils of lipid-conjugated Aβ(1–40) peptides are somewhat more heterogeneous than wildtype Aβ fibrils.

Most interestingly, the ^{13}C solid-state NMR results reveal that a significant reorganization of the N-terminal part of the Aβ hybrids occurs. Drastic ^{13}C NMR chemical shift changes of Ala$_2$ and Phe$_4$ indicate that the N-terminus undergoes a structural change from random coil in wildtype Aβ(1–40) to a well-defined β-sheet structure. Furthermore, the segmental order parameter for the Cα–H bond vector of Ala$_2$ increases from 0.65 in unmodified Aβ to 0.9 in the two lipid-conjugated peptides. The order parameter of Phe$_4$ in palmitoyl–Aβ(1–40) increases to 0.85 compared to 0.61 in wildtype Aβ fibrils. This means that the amplitudes of the fluctuations, the ^{1}H–^{13}Cα bond vectors in the N-terminus of the lipid-conjugated Aβ fibrils undergo, are significantly reduced. Furthermore, there appears to be a very steep gradient in the amplitude of the molecular fluctuations from the N-terminal residues to the lipid segments of the lipid chains. The structuring of the N-terminus of Aβ as well as the assembly of the lipid modification does not depend on the length of the lipid chain attached to the peptide.

The structure of the core of the Aβ fibril is not influenced by the N-terminal lipid conjugation. Nevertheless, the investigated amino acids of the fibril core experience a substantial increase in their order parameters, indicating a more compact packing of the fibrils. The turn region, which was probed by Gly$_{25}$, however, remained uninfluenced by the N-terminal lipid modification.

1844 | *Phys. Chem. Chem. Phys.*, 2017, **19**, 1839–1846

This journal is © the Owner Societies 2017

Apparently, the energy landscape of Aβ misfolding is modified by the solvent conditions or the hydrophobicity of the entire molecule, which can lead to more or less extended cross-β structures.

Implications of our findings can be found, for instance, in the biologically relevant interaction of amyloid forming protein with biological membranes.[47] As proteins that form amyloids typically consist of a fibril part, organized in the cross-β structure, and unstructured flexible segments that flank the core of the fibrils,[48–50] the extent of β-structure may vary significantly in the vicinity of membrane surfaces. This may also lead to tertiary structure changes of the Aβ amyloids, which could be relevant with regard to their toxic effects on neurons by disrupting the cellular membranes.[51]

In conclusion, we investigated the interplay between lipid assembly *versus* amyloid structure formation in hybrid molecules of lipid conjugated Aβ peptides. The results show that cross-β structure formation is accelerated for the more hydrophobic N-termini of the Aβ peptides. This suggests that amyloid formation is the dominating structure forming mechanism in these lipid-modified Aβ peptides. The lipid moieties on the N-terminus show a tendency for a dynamic heterogeneous lipid assembly that is loosely structured. The association of the lipidated N-termini induces largely immobilized β-strand structure at least for the first amino acids of the Aβ N-terminus. However, this likely fibrillar structure is also heterogeneous. This suggests that the extent of the cross-β structure found in amyloids sensitively depends on local hydrophobicity imposed onto the sequence. This supports the high fibrillation capacity of Aβ peptides that can apparently also extend towards the N-terminus if it is constraint by formation of an aggregated lipid phase.

Acknowledgements

References

1 S. Drotleff, U. Lungwitz, M. Breunig, A. Dennis, T. Blunk, J. Tessmar and A. Gopferich, *Eur. J. Pharm. Biopharm.*, 2004, **58**, 385.

2 H. A. Klok, *Macromolecules*, 2009, **42**, 7990.

3 A. Rosler, H. A. Klok, I. W. Hamley, V. Castelletto and O. O. Mykhaylyk, *Biomacromolecules*, 2003, **4**, 859.

4 H. A. Klok and S. Lecommandoux, *Adv. Mater.*, 2001, **13**, 1217.

5 F. Chiti and C. M. Dobson, *Annu. Rev. Biochem.*, 2006, **75**, 333.

6 I. W. Hamley, *Chem. Rev.*, 2012, **112**, 5147.

7 R. Tycko, *Protein Sci.*, 2014, **23**, 1528.

8 M. A. Walti, F. Ravotti, H. Arai, C. G. Glabe, J. S. Wall, A. Bockmann, P. Guntert, B. H. Meier and R. Riek, *Proc. Natl. Acad. Sci. U. S. A.*, 2016, **113**, E4976.

9 M. T. Colvin, R. Silvers, Q. Z. Ni, T. V. Can, I. Sergeyev, M. Rosay, K. J. Donovan, B. Michael, J. Wall, S. Linse and R. G. Griffin, *J. Am. Chem. Soc.*, 2016, **138**, 9663.

10 Y. Xiao, B. Ma, D. McElheny, S. Parthasarathy, F. Long, M. Hoshi, R. Nussinov and Y. Ishii, *Nat. Struct. Mol. Biol.*, 2015, **22**, 499.

11 Z. Ge and S. Liu, *Chem. Soc. Rev.*, 2013, **42**, 7289.

12 X. Fan, Y. Zhao, W. Xu and L. Li, *Mater. Sci. Eng., C*, 2016, **62**, 943.

13 C. Ginn, H. Khalili, R. Lever and S. Brocchini, *Future Med. Chem.*, 2014, **6**, 1829.

14 I. W. Hamley and M. J. Krysmann, *Langmuir*, 2008, **24**, 8210.

15 A. Rosler, H. A. Klok, I. W. Hamley, V. Castelletto and O. O. Mykhaylyk, *Biomacromolecules*, 2003, **4**, 859.

16 T. S. Burkoth, T. L. Benzinger, D. N. M. Jones, K. Hallenga, S. C. Meredith and D. G. Lynn, *J. Am. Chem. Soc.*, 1998, **120**, 7655.

17 T. S. Burkoth, T. L. Benzinger, V. Urban, D. G. Lynn, S. C. Meredith and P. Thiyagarajan, *J. Am. Chem. Soc.*, 1998, **121**, 7429–7430.

18 V. Castelletto, G. E. Newby, Z. Zhu, I. W. Hamley and L. Noirez, *Langmuir*, 2010, **26**, 9986.

19 S. Dehn, V. Castelletto, I. W. Hamley and S. Perrier, *Biomacromolecules*, 2012, **13**, 2739.

20 G. Reuther, K.-T. Tan, J. Köhler, C. Nowak, A. Pampel, K. Arnold, J. Kuhlmann, H. Waldmann and D. Huster, *Angew. Chem., Int. Ed.*, 2006, **45**, 5387.

21 L. Brunsveld, H. Waldmann and D. Huster, *Biochim. Biophys. Acta*, 2009, **1788**, 273.

22 P. J. Casey, *Science*, 1995, **268**, 221.

23 R. Nelson, M. R. Sawaya, M. Balbirnie, A. O. Madsen, C. Riekel, R. Grothe and D. Eisenberg, *Nature*, 2005, **435**, 773.

24 J. Adler, H. A. Scheidt, M. Kruger, L. Thomas and D. Huster, *Phys. Chem. Chem. Phys.*, 2014, **16**, 7461.

25 J. Adler, M. Baumann, B. Voigt, H. A. Scheidt, D. Bhowmik, T. Haupl, B. Abel, P. K. Madhu, J. Balbach, S. Maiti and D. Huster, *ChemPhysChem*, 2016, **17**, 2744.

26 C. Tanford, *The Hydrophobic Effect: Formation of Micelles and Biological Membranes*, John Wiley & Sons, New York, 1980, ch. 3, pp. 14–20.

27 A. Vogel, C. P. Katzka, H. Waldmann, K. Arnold, M. F. Brown and D. Huster, *J. Am. Chem. Soc.*, 2005, **127**, 12263.

28 H. A. Scheidt, I. Morgado, S. Rothemund and D. Huster, *J. Biol. Chem.*, 2012, **287**, 2017.

29 E. London and G. W. Feigenson, *Biochemistry*, 1981, **20**, 1939.

30 P. Khuwijitjaru, S. Adachi and R. Matsuno, *Biosci., Biotechnol., Biochem.*, 2002, **66**, 1723.

31 P. S. Vassar and C. F. Culling, *Arch. Pathol.*, 1959, **68**, 487.

32 L. Nielsen, R. Khurana, A. Coats, S. Frokjaer, J. Brange, S. Vyas, V. N. Uversky and A. L. Fink, *Biochemistry*, 2001, **40**, 6036.

33 J. H. Davis, K. R. Jeffrey, M. Bloom, M. I. Valic and T. P. Higgs, *Chem. Phys. Lett.*, 1976, **42**, 390.

This journal is © the Owner Societies 2017

Phys. Chem. Chem. Phys., 2017, **19**, 1839–1846 | **1845**

34 T. Gopinath and G. Veglia, *Angew. Chem., Int. Ed.*, 2012, **51**, 2731.

35 M. G. Munowitz, R. G. Griffin, G. Bodenhausen and T. H. Huang, *J. Am. Chem. Soc.*, 1981, **103**, 2529.

36 A. Bielecki, A. C. Kolbert and M. H. Levitt, *Chem. Phys. Lett.*, 1989, **155**, 341.

37 P. Barré, O. Zschörnig, K. Arnold and D. Huster, *Biochemistry*, 2003, **42**, 8377.

38 D. Huster, *Prog. Nucl. Magn. Reson. Spectrosc.*, 2005, **46**, 79.

39 L. Nielsen, R. Khurana, A. Coats, S. Frokjaer, J. Brange, S. Vyas, V. N. Uversky and A. L. Fink, *Biochemistry*, 2001, **40**, 6036.

40 M. Sunde, L. C. Serpell, M. Bartlam, P. E. Fraser, M. B. Pepys and C. C. Blake, *J. Mol. Biol.*, 1997, **273**, 729.

41 G. D. Henry and B. D. Sykes, *Methods Enzymol.*, 1994, **239**, 515.

42 J. Seelig, *Q. Rev. Biophys.*, 1977, **10**, 353.

43 J. H. Davis, *Biochim. Biophys. Acta*, 1983, **737**, 117.

44 S. Stahlberg, B. Skolova, P. K. Madhu, A. Vogel, K. Vavrova and D. Huster, *Langmuir*, 2015, **31**, 4906.

45 R. E. Stark, J. L. Manstein, W. Curatolo and B. Sears, *Biochemistry*, 1983, **22**, 2486.

46 H. A. Scheidt, A. Sickert, T. Meier, N. Castellucci, C. Tomasini and D. Huster, *Org. Biomol. Chem.*, 2011, **9**, 6998.

47 C. Galvagnion, J. W. Brown, M. M. Ouberai, P. Flagmeier, M. Vendruscolo, A. K. Buell, E. Sparr and C. M. Dobson, *Proc. Natl. Acad. Sci. U. S. A.*, 2016, **113**, 7065.

48 M. Sackewitz, H. A. Scheidt, G. Lodderstedt, A. Schierhorn, E. Schwarz and D. Huster, *J. Am. Chem. Soc.*, 2008, **130**, 7172.

49 H. Heise, W. Hoyer, S. Becker, O. C. Andronesi, D. Riedel and M. Baldus, *Proc. Natl. Acad. Sci. U. S. A.*, 2005, **102**, 15871.

50 M. Gopalswamy, A. Kumar, J. Adler, M. Baumann, M. Henze, S. T. Kumar, M. Fandrich, H. A. Scheidt, D. Huster and J. Balbach, *Biochim. Biophys. Acta*, 2015, **1854**, 249.

51 M. F. Sciacca, J. R. Brender, D. K. Lee and A. Ramamoorthy, *Biochemistry*, 2012, **51**, 7676.

1846 | *Phys. Chem. Chem. Phys.*, 2017, **19**, 1839–1846

This journal is © the Owner Societies 2017